

PFC/RR-92-8

DOE/PC-90350-5

**DC CICC Retrofit Magnet  
Preliminary Design,  
Software Development and Analysis Report**

Quarterly Progress Report  
Contract No. DE-FG22-90PC90350  
April 1992

R. Leonard Myatt and P.G. Marsion

Submitted May 28, 1992

Massachusetts Institute of Technology  
Plasma Fusion Center  
175 Albany Street  
Cambridge, MA 02159

## **1.0 Introduction**

The January 1992 quarterly progress report<sup>1</sup> discusses a two-dimensional finite element analysis (FEA) of the proposed retrofit MHD coil. The superconducting Cable-in-Conduit Conductor (CICC) winding pack has a smooth, semi-elliptical cross section and is supported by a similarly shaped strap which resists the electromagnetic forces tending to separate the coils on each side of the channel. The coils are designed to produce a peak on-axis field of 4.5 tesla with a nominal current density of  $13.05 \times 10^6$  A/m<sup>2</sup>. A sketch of the magnet system and structure is shown in Fig. 1.0-1.

The objective of this analysis is to quantify the highly 3-D characteristics of the proposed superconducting magnet system, and develop an appropriate support concept. A fully paramatized 3-D finite element model of the coil and structure is developed as a means of obtaining the field and stress solutions. The flexibility of FEA and a model built using design parameters allows variations in the coil end turn bend radius, strap thickness, support details and positions to be studied. The preliminary results show the calculated stresses as a result of this iterative design process.

## **2.0 Summary and Conclusions**

The detailed finite element analysis presented here verifies the credibility of the proposed constant tension support concept for the DC CICC retrofit MHD magnet. Stresses in the structural members are on the order of 100 to 200 MPa, which are reasonable for the materials being considered. Regions of higher stress can be accommodated by subtle modifications and refinements to the structure, and more detailed analysis. However, at this stage of design and analysis, the fundamental structural requirements are met by the proposed design.

## **3.0 Analysis Description**

The analysis described here is designed to evaluate the complex 3-D behavior of the dipole coil and support structure. The electromagnetic and structural evaluations are based on a 3-D nonlinear finite element analysis of the proposed MHD coil and support concept. The finite element model ignores the slight taper in the magnet system which allows the use of three symmetry planes thereby greatly reducing the model size and computational time.

### **3.1 The Finite Element Model**

The winding pack cross section with a nominal build of 0.72 meter width and 0.88 meter half height represents a coil which operates right at the design current density of about 13 MA-turns/m<sup>2</sup>. The analysis assumes zero friction between the coil and the strap. Although not entirely true, this assumption is necessary due to the size and complexity of the 3-D nonlinear model. The ref. 1 report discusses the effects of friction on the stresses in the coil, and indicates that relative motion between the strap and the coil is an essential part of the design concept.

The model is generated within the ANSYS PREP7 preprocessor. Fundamental dimensions are defined by parameters which greatly simplify the inevitable changes to the model which occur during the design and analysis process. Changes such as mesh density, coil build, end turn support plate thicknesses and crossover radii can all be accommodated by simply redefining numbers in the parameter list. Figures 3.1-1 to 3.1-3 show the finite element model in some detail.

### 3.2 Material Properties

The nature of the analysis and its objectives establish the level of detail that must be included in the model. On this basis, the actual winding pack (i.e., insulation, conductor, conduit) is approximated by smeared orthotropic material properties.

Modulus of Elasticity:

$$\begin{aligned} E_x = E_z &= 28 \text{ GPa (Transverse)} \\ E_y &= 58 \text{ GPa (Longitudinal)} \end{aligned}$$

Shear Modulus:

$$\begin{aligned} G_{xy} &= 7 \text{ GPa (Trans-Long)} \\ G_{yz} &= 20 \text{ GPa (Long-Trans)} \\ G_{xz} &= 9 \text{ GPa (Trans-Trans)} \end{aligned}$$

Poisson's Ratio:

$$\begin{aligned} \nu_{xy} &= 0.30 \text{ (Trans Strain from Long Stress)} \\ \nu_{yz} &= 0.16 \text{ (Long Strain from Trans Stress)} \\ \nu_{xz} &= 0.24 \text{ (Trans Strain from Trans Stress)} \end{aligned}$$

These properties are calculated such that the global structural characteristics of the saddle coil are represented. The material properties associated with the strap, end turn support plates, and gussets are simply isotropic constants.

### 3.3 Boundary Conditions and Solution Process

Displacement boundary conditions for the structural analysis provide for full machine behavior by specifying zero displacements across the three symmetry planes. The model is loaded electromagnetically by a uniform current density of  $13.05 \times 10^6 \text{ A/m}^2$ , which produces a nominal 4.5 tesla at the machine axis. The first pass of the analysis solves the electrical problem. One end of the coil is set to zero potential, while a known current is applied at the other. The current density is essentially uniform across the build of the coil, as it must be in a superconducting application. The second pass of the analysis solves the magnetics problem.  $J \times B$  body forces are also calculated and saved automatically as input to the next pass of the analysis which is the structural solution. The analysis is complete when the nonlinear gap elements have converged as the coil strains and slips within the confines of the supporting structure.

### 3.4 Structural Details

During the coil manufacturing process, the conductor is bent to form the end turns of the magnet. Plastic deformation occurs, which is often called keystoneing as it describes the shape of the deformed cross section (see Fig 3.4-1). The amount of distortion is inversely proportional to the bend radius. For large radii, the effect is small and the distortion is minimal. An end turn with a large bend radius is inefficient as it consumes valuable space and material, and locally degrades the quality of the magnetic field. An end turn with a small bend radius is compact and efficient, but results in an array of oddly shaped conductors which, as a result, load and strain with non-uniformities. Therefore, establishing a minimum bend radius requires striking a compromise. The permanent strain ( $\delta$ ) can be quantified by the following simple equation:

$$\delta = t^2 / 8r$$

where  $t$  is the thickness of the conduit, and  $r$  is the bend radius. The maximum deformation is chosen to be 0.5 mm, which establishes a minimum bend radius of about 30 cm.

Although the conductor winding pack represents a significant structural cross section, the electromagnetic forces in the end turn region are high and tend to collapse the opposing coils. These forces are resisted by reinforced support plates which are located under the end turn winding packs. The construction of these plates is limited locally by the distance between the coil and the channel. Outboard of the channel the plates are well reinforced by gussets which span the distance between the two end turns. This support concept is shown in the CAD drawing of Fig 3.4-2.

### 4.0 Results

The results of the analysis are best summarized by the graphical output from the computer finite element model. The following is a series of plots depicting the stresses in the various components of the system.

Figure 4.0-1 shows the tresca stress intensity in the support shell, which extends the length of the straight section and into the first bend region of the end turn. The nominal stress in the 2" thick shell is about 150 MPa, and peaks to 270 MPa in a very small localized region at the tight bend. This high stress can be relieved by altering the structure in that particular region.

Figure 4.0-2 shows the tresca stress intensity in the shell extension. Ignoring the region where the shell tapers to a knife edge, all the stresses are also 150 MPa and below.

Figure 4.0-3 shows the stresses in the end turn support plate which carries the winding pack up and over the channel. The vast majority of stresses within the structure are below 200 MPa. As with the shell extension, there is a local region of high stress due to the sharp taper where the two coils diverge to form the end turn.

Figure 4.0-4 shows the tresca stress intensity in the gusset plates which bridge the span between the upper and lower support plates at each end of the magnet system. The stresses shown here are all below 100 MPa, and pose no threat to the structural integrity of the design.

However, in the actual design, these plates are joined and closed off by a cover plate, adding rigidity and stability to an otherwise open section.

Figure 4.0-5 shows the tresca stress intensity in the aluminum sheath, the structural element of the conductor winding pack. At the magnet midplane the stresses match those of the 2-D analysis of reference 1. Stresses peak at about 110 MPa in the transition region between the end turn and straight section. Stresses at the end turn mid-span, directly above the channel centerline, peak at about 80 MPa, an indication that the end turns are well supported by the gusseted plate design presented here.

## **5.0 References**

1. R.Leonard Myatt and P.G. Marston, "DC CICC Retrofit Magnet Preliminary Design, Software Development and Analysis Report," DOE/PC-90350-4, Submitted February 10, 1992, MOT Plasma Fusion Center, Cambridge, MA

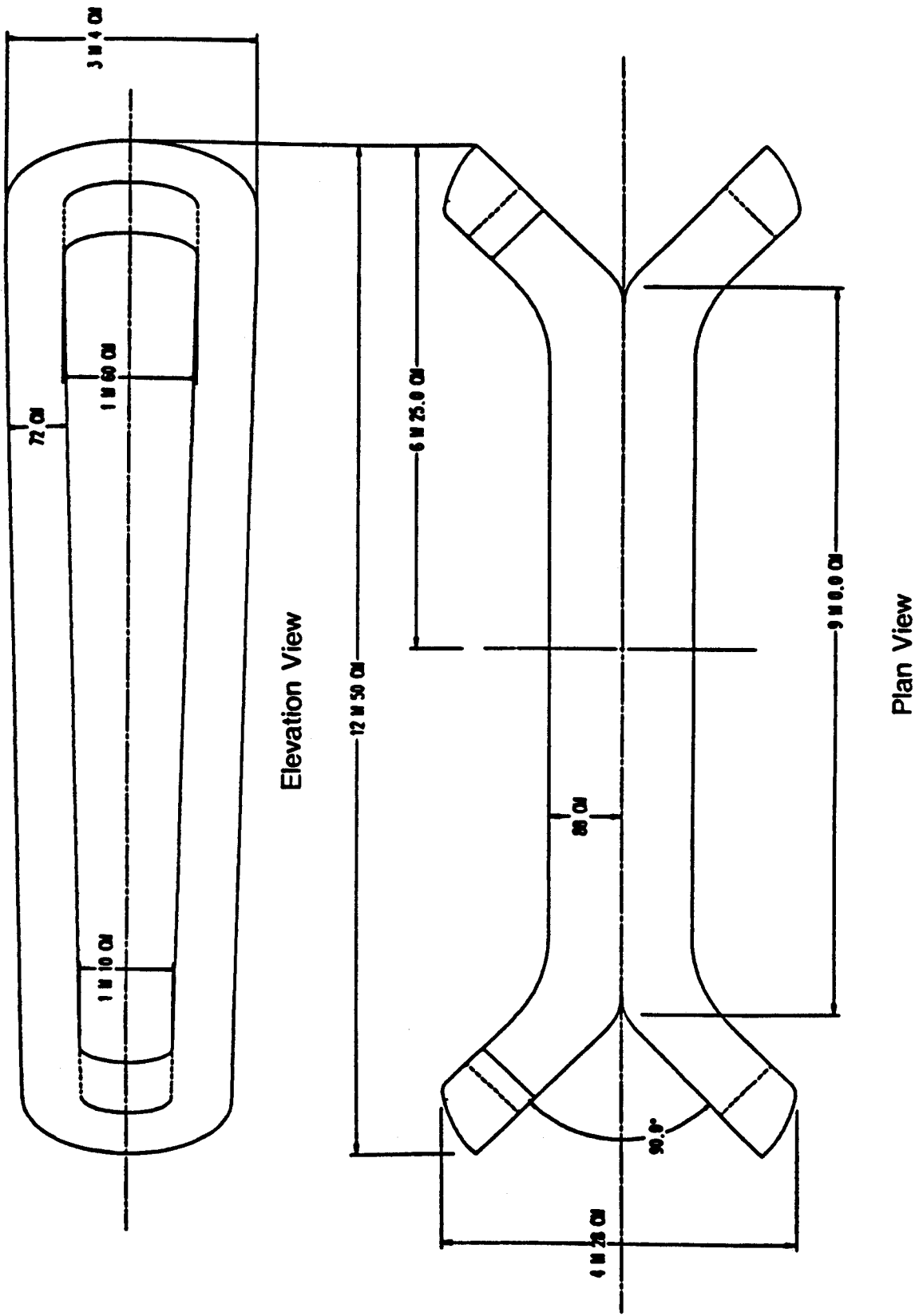


Fig 1.0-1 Nominal Magnet Geometry

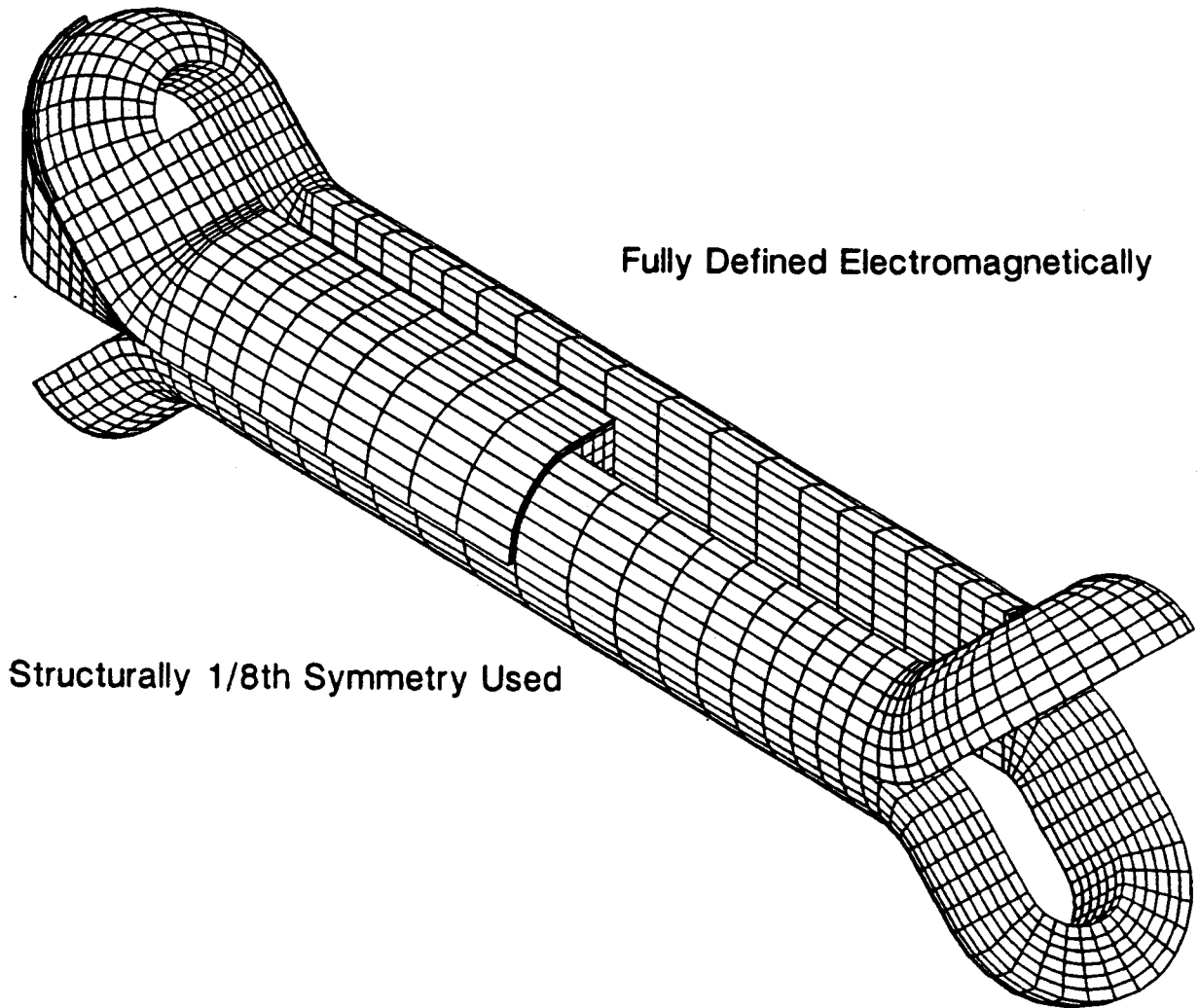


Fig 3.1-1 ANSYS 3-D Finite Element Model

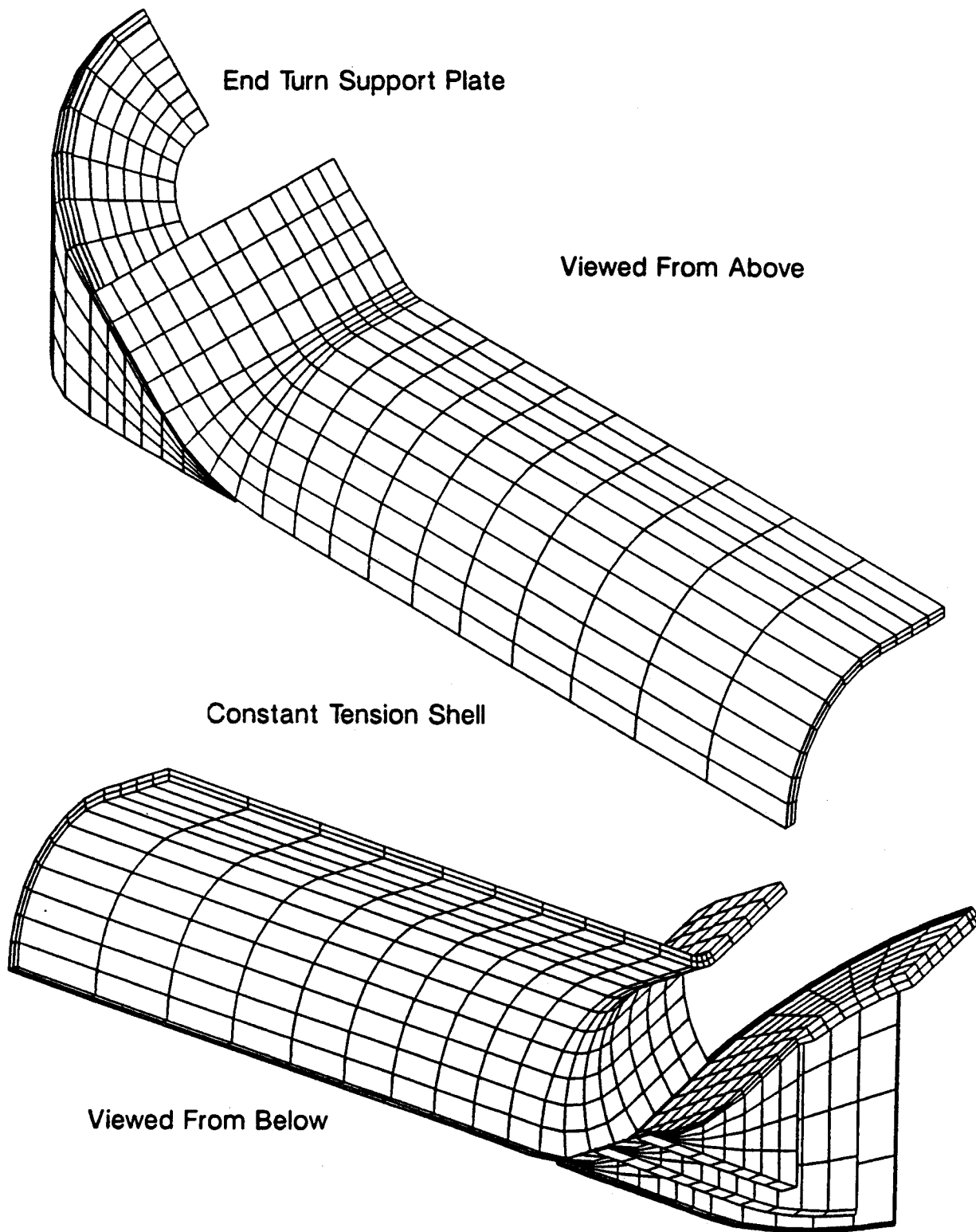


Fig 3.1-2 Support Structure Isometrics

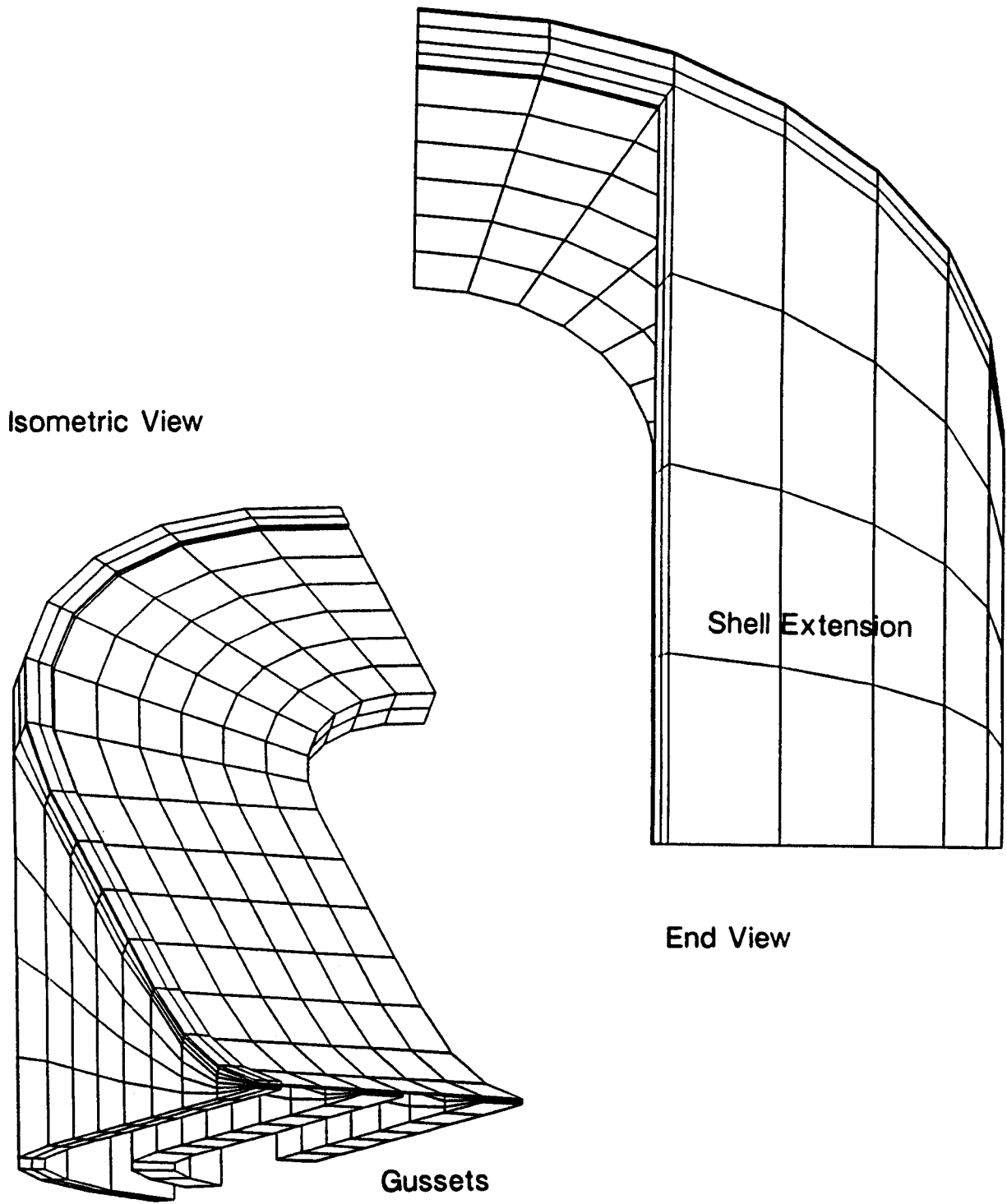


Fig 3.1-3 End Turn Support

ANSYS 4.4A

APR 7 1992

9:40:42

PLOT NO. 1

POST1 DISPL.

STEP=1

ITER=1

DMX =0.413E-03

ERPC=24.695

DSCA=4.792

ZV =1

DIST=0.0198

YF =0.009

ZF =0.491E-03

Bent About Y-Axis, Center of Curvature at X=-23 cm

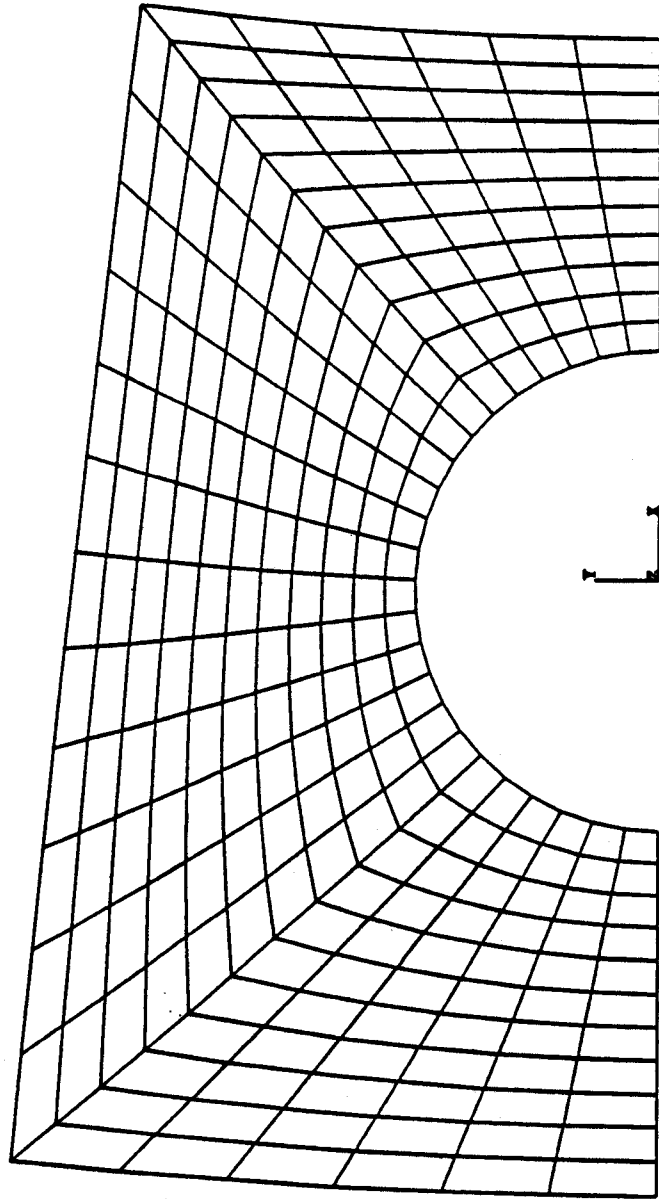


Fig 3.4-1 Conductor Cross Section Deformed by Bending

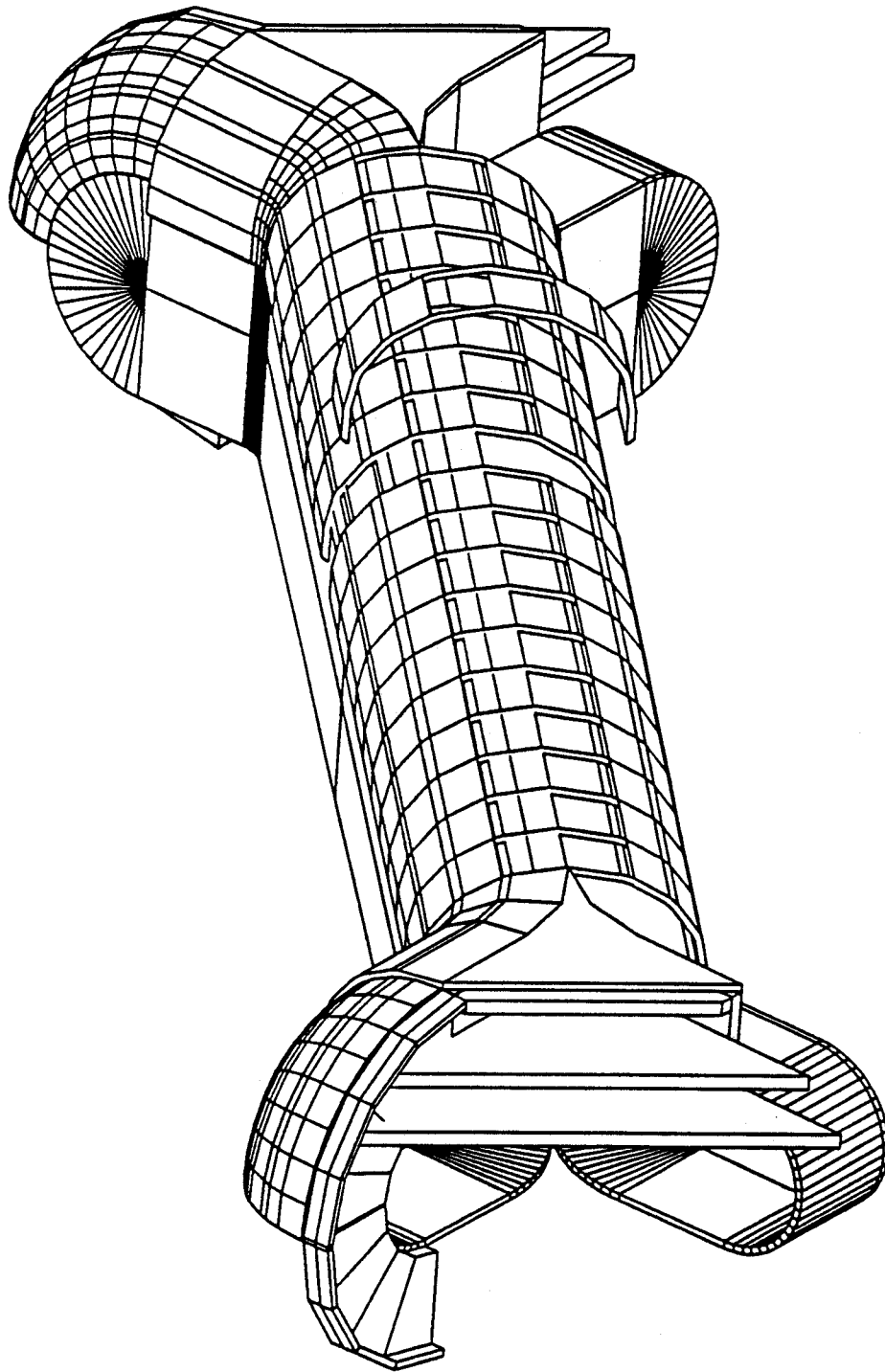


Fig 3.4-2 CAD Drawing of Proposed Structure

ANSYS 4.4A

APR 4 1992

7:30:07

PLOT NO. 1

POST1 STRESS

STEP-1

ITER-5

SI (AVG)

DMX -0.002078

SMN -0.109E+08

SMX -0.273E+09

XV -1

YV -1

DIST-3.266

XF -0.66415

YF -0.806739

ZF -2.969

PRECISE HIDDEN

A -0.255E+08

B -0.546E+08

C -0.837E+08

D -0.113E+09

E -0.142E+09

F -0.171E+09

G -0.200E+09

H -0.229E+09

I -0.258E+09

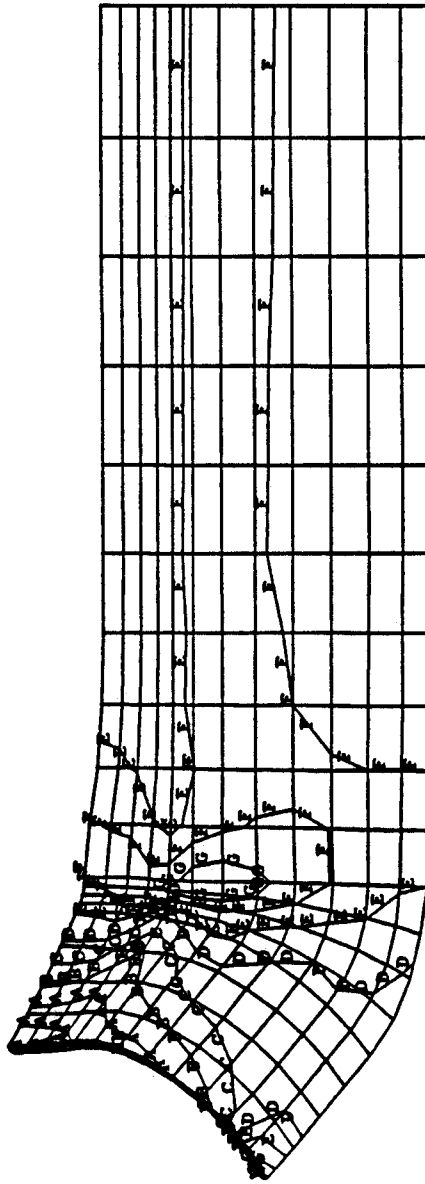


Fig 4.0-1 Stress Contours in Constant Tension Shell [Pa]

ANSYS 4.4A

APR 4 1992

7:30:51

PLOT NO. 5

POST1 STRESS

STEP-1

ITER-5

SI (AVG)

DMX -0.001779

SMN -0.877E+07

SMX -0.213E+09

XV -1

YV -0.5

ZV -0.5

DIST-1.238

XF -0.941293

YF -0.859545

ZF -5.797

PRECISE HIDDEN

A -0.201E+08

B -0.428E+08

C -0.655E+08

D -0.882E+08

E -0.111E+09

F -0.134E+09

G -0.156E+09

H -0.179E+09

I -0.202E+09

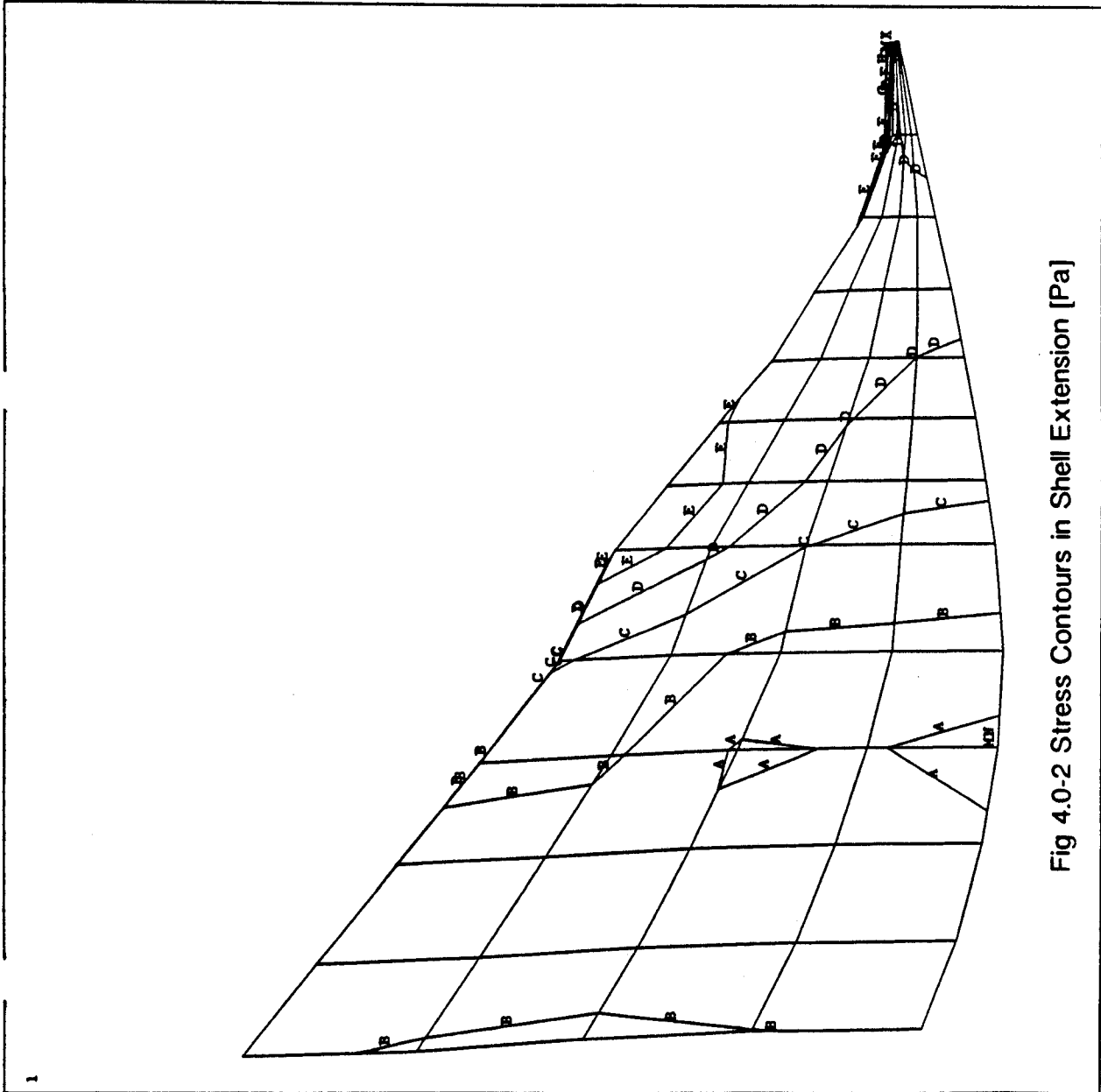


Fig 4.0-2 Stress Contours in Shell Extension [Pa]

ANYSYS 4.4A

APR 4 1992

7:30:33

PLOT NO. 3

POST1 STRESS

STEP-1

ITER-5

S1 (AVG)

DMX -0.001747

SME -0.799E+07

SMX -0.642E+09

TV -1

TV -1

DIST-1.993

XF -0.66415

YF -0.947079

ZF -5.843

PRECISE MIDDEN

A -0.432E+08

B -0.114E+09

C -0.184E+09

D -0.254E+09

E -0.325E+09

F -0.395E+09

G -0.466E+09

H -0.536E+09

I -0.606E+09

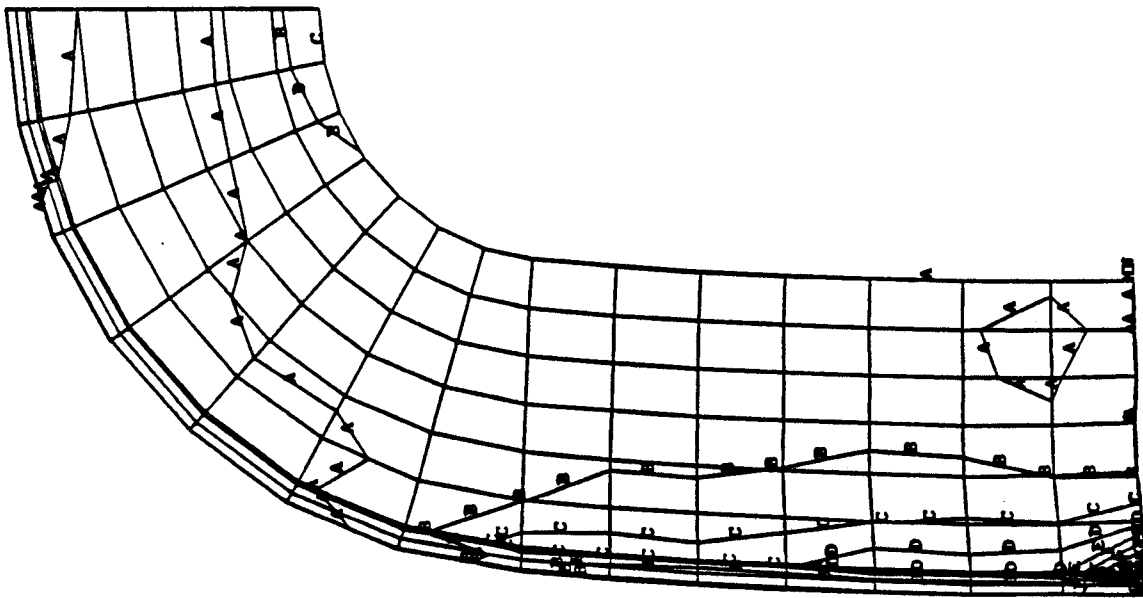


Fig 4.0-3 Stress Contours in End Turn Support Plate [Pa]

ANSYS 4.4A

APR 4 1992

7:30:43

PLOT NO. 4

POST1 STRESS

STEP-1

ITER-5

SI (AVG)

DMX -0.001742

SMN -0.359E+07

SMX -0.105E+09

XV --1

YV -1

ZV --1

DIST-1.172

XF -0.79

YF -0.721139

ZF -5.659

PRECISE HIDDEN

A -0.923E+07

B -0.205E+08

C -0.318E+08

D -0.430E+08

E -0.543E+08

F -0.656E+08

G -0.768E+08

H -0.881E+08

I -0.994E+08

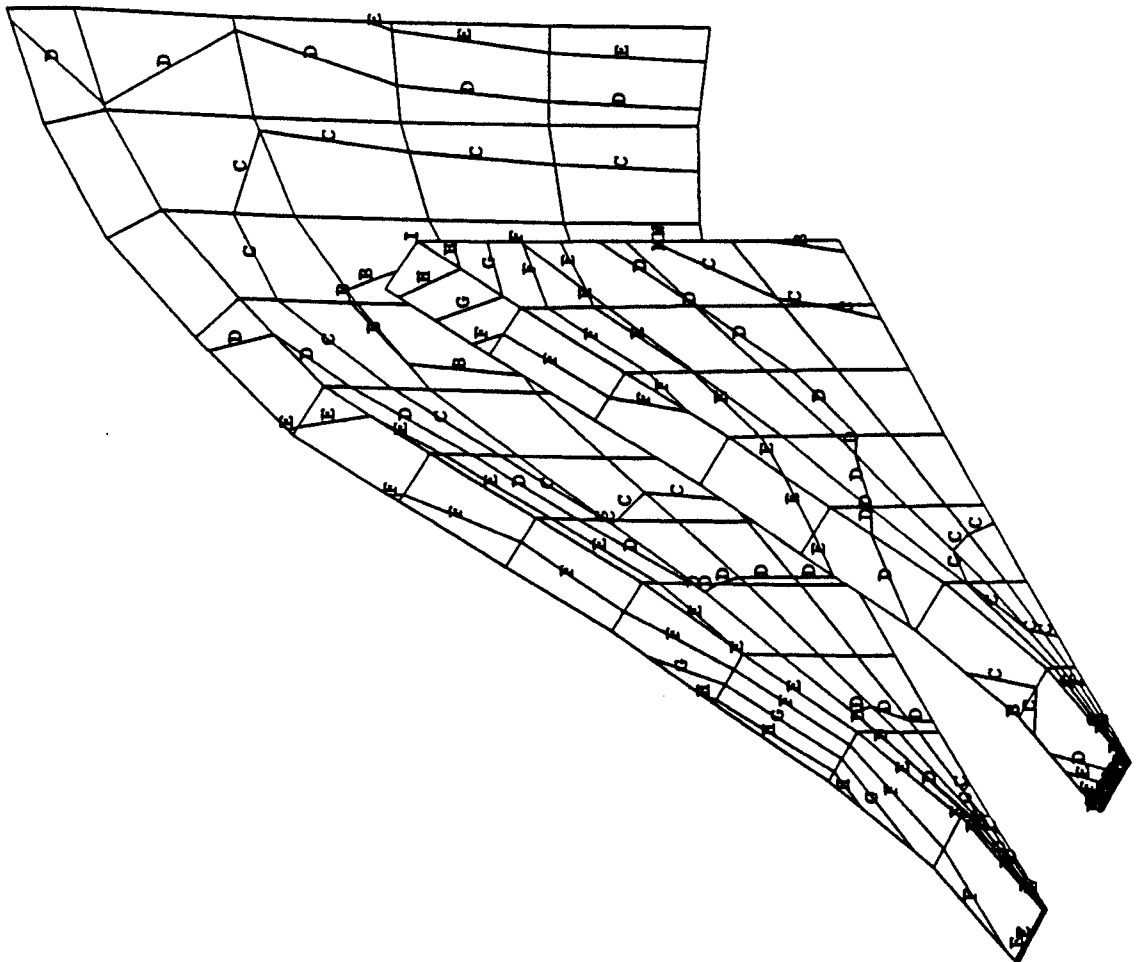


Fig 4.0-4 Stress Contours in End Turn Gusset Plates [Pa]

AMSTS 4.4A

APR 4 1992

7:32:25

PLOT NO. 10

POST1 STRESS

STEP=1

ITER=5

S23 (AVG)

DMX -0.002481

SMN -0.165E+07

SMX -0.109E+09

XV --1

YV -1

ZV --1

DIST=3.153

XF -0.635

YF -1.071

ZF -3.418

PRECISE HIDDEN

A -0.760E+07

B -0.195E+08

C -0.314E+08

D -0.433E+08

E -0.552E+08

F -0.671E+08

G -0.790E+08

H -0.909E+08

I -0.103E+09

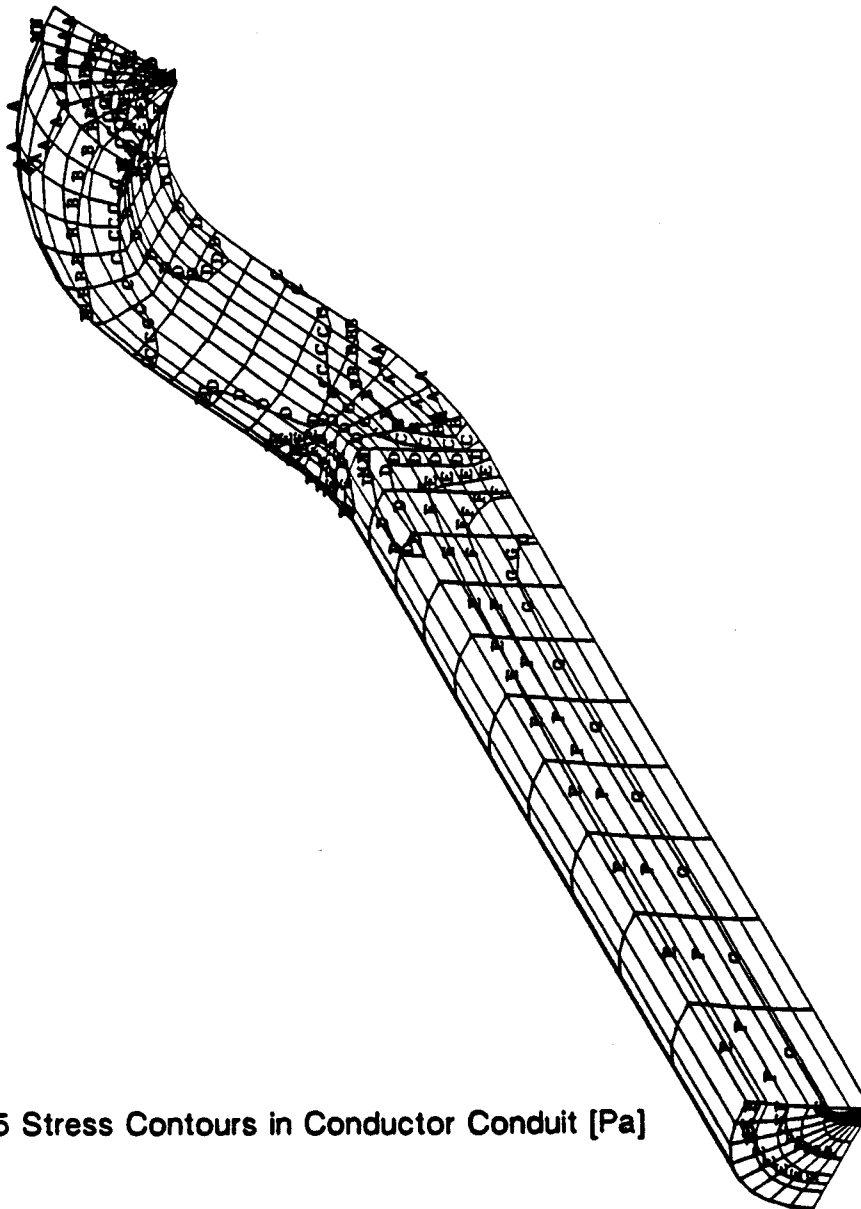


Fig 4.0-5 Stress Contours in Conductor Conduit [Pa]